



Atmospheric Plasma Spraying of Different MgO/Al₂O₃ Feedstocks

Robert Vaßen¹ · Tobias Kalfhaus¹ · Christoph Vorkötter¹ · Yoo Jung Sohn¹ · Susan Conze² · Lutz-Michael Berger²

Submitted: 8 September 2022 / in revised form: 22 November 2022 / Accepted: 1 January 2023 / Published online: 2 February 2023
© The Author(s) 2023

Abstract Nine commercial and experimental powders from the MgO/Al₂O₃ system have been investigated in the present project. The composition ranged from MgO/MgAl₂O₄ composites with more than 70% MgO to an alumina-rich spinel powder (94% Al₂O₃). The powders were fused and crushed or agglomerated and sintered. The influence of the composition, the manufacturing route as well as the particle size distribution on the microstructure and the phases in the produced coatings have been investigated. For several of the powders, detailed design of experiment plans have been made and properties such as deposition efficiency, hardness and porosity were optimized. With optimized spray conditions coatings have been produced from all powders which were characterized in depth. Here, the results of microstructure, porosity values and thermal cyclic tests will be presented in more detail.

Keywords abradable coating · applications · electrical insulation · high temperature application

Introduction

Magnesium aluminum spinel (MgAl₂O₄) is a ceramic material with a large number of interesting properties as high temperature stability, good mechanical properties, high electrical resistance and good catalytic behavior at reasonable costs (Ref 1). These properties led to different applications of the bulk spinel material, e.g., as refractory replacing the more toxic magnesia chrome bricks in kiln applications.

As the material shows congruent melting, it is also feasible for the deposition by thermal spraying. However, not many investigations on this processing route are found in the literature although the powder is already commercially available since several decades (Ref 2). A couple of applications of spinel coatings have been reported in the past. In particular, in the case of high temperature coatings, a number of investigations are found in the literature (Ref 3). One investigation showed the high temperature stability of spinels — especially the high sintering resistance — which is interesting for thermal barrier coating applications, although the thermal conductivity is not very low. Columnar structured thermal barrier coatings produced by suspension plasma spraying showed very attractive thermal cycling behavior (Ref 4). This paper also details on the relation of the lattice parameter and the stoichiometry factor describing the ratio of MgO and Al₂O₃ given for plasma-sprayed coatings.

The good stability and moderate thermal conductivity made the MgAl₂O₄ spinels an ideal candidate for abradable seals of high-pressure turbines in aeroengines (Ref 5).

This article is an invited paper selected from presentations at the 2022 International Thermal Spray Conference, held May 4–6, 2022, in Vienna, Austria, and has been expanded from the original presentation. The issue was organized by André McDonald, University of Alberta (Lead Editor); Yuk-Chiu Lau, General Electric Power; Fardad Azarmi, North Dakota State University; Filofteia-Laura Toma, Fraunhofer Institute for Material and Beam Technology; Heli Koivuluoto, Tampere University; Jan Cizek, Institute of Plasma Physics, Czech Academy of Sciences; Emine Bakan, Forschungszentrum Jülich GmbH; Šárka Houdková, University of West Bohemia; and Hua Li, Ningbo Institute of Materials Technology and Engineering, CAS.

✉ Robert Vaßen
r.vassen@fz-juelich.de

¹ Forschungszentrum Jülich GmbH, IEK-1, 52425 Jülich, Germany

² Fraunhofer IKTS, Winterbergstr 28, 01277 Dresden, Germany

Thick coatings in the millimeter range have been applied by atmospheric plasma spraying (APS) (Ref 6).

Furthermore, spinels can also be used to manufacture free-standing ceramic bodies by thermal spray technologies. These components offer excellent thermal shock resistance due to the specific microstructure in combination with the material properties (Ref 7).

Spinel coatings have also been investigated for applications where contact with liquid metals occurs as in foundries. An older work describes the reaction with Al/Si melts (Ref 8), another applications in the steel industry (Ref 9). Moreover, these coatings were tested for application in fusion reactors (Ref 10). In a more recent work, plasma-sprayed spinel coatings have been used as potential barrier coatings in future fast reactors (FFRs) being in direct contact with liquid sodium at 400 °C for 1000 h (Ref 11).

The electrical insulative properties of the spinel coatings make it also attractive for different functional applications, for example, it has been used to manufacture humidity sensors (Ref 12–14). Another application is insulative coatings on metallic interconnects of solid oxide fuel cells applied by vacuum plasma spraying (Ref 15).

The listed examples show that there are already a number of applications for spinel coatings, and however, in-depth investigations on the coating development are missing. Only very few reports are found in the literature on the development of thermally sprayed spinel coatings as the one of Lallemand (Ref 16).

So, in the present investigation, commercially available powders with compositions close to the stoichiometric one as well as experimental powders with higher MgO or Al₂O₃ contents, respectively, were used. The focus of the coating development was the manufacture of dense coatings. Porosity values and deposition efficiencies were evaluated in design of experiments (DOE) for three powders. Optimized conditions were used to spray all nine powders to investigate the microstructure (phase analysis and porosity levels) as well as the mechanical (hardness) and functional properties. Finally, thermal cyclic performance is presented as well.

Experimental

A selection of three different commercially available MgO-Al₂O₃ feedstock powders and six experimental powders were used in this study. The different powders are listed in Table 1. The d10/d50/d90 values of the particle size distributions were determined by laser diffraction (Horiba LA-950-V2).

All feedstock powders were characterized in detail. Bulk and tap densities were measured. A Bruker D4 Endeavor

was employed to determine phase contents of each powder via x-ray diffraction (XRD). Each diffraction pattern was recorded in a range of $2\Theta = 10\text{--}80^\circ$ with a step size of 0.02° and a measurement time of 2 s per step in a simultaneous measurement range of 4° . Phase quantification was then performed by Rietveld refinement using the TOPAS Software.

Atmospheric plasma spraying (APS) was used to produce coatings with thicknesses of several 100 µm with exception of the low-density powders with reduced thickness values below 200 µm. An Oerlikon Metco F4 plasma torch with a nozzle diameter of 6 mm was used in an Oerlikon Metco Multicoat System. For the detailed design of experiment (DoE) investigation, three powders were selected. One commercial stoichiometric fused and crushed powder (072fc-a1) as well as one commercial agglomerated and sintered powder (076as-a) and one experimental powder with high amount of alumina (094fc-a) were selected. The design of experiment (DoE) plan was a Box–Behnken one; the used parameters are shown in Table 2. The Box–Behnken design plan allows an efficient evaluation of quadratic models using three levels including a center point. This is measured two times, at the beginning and the end of the spray trials. 12 different parameters with the double center point double were used. The influence of these parameters on the deposition efficiency, porosity, and hardness was evaluated. The identified optimal deposition parameters were also used to prepare coatings from all the other powders.

The surface speed of the torch was set to 1000 mm/s. Prior to spraying, each grit-blasted mild steel substrate ($30 \times 25 \times 4 \text{ mm}^3$) was preheated to about 120 °C. During spraying, the substrate was cooled by air jets. The feed rate of each powder was determined at the beginning of the spraying experiments. This feed rate was then used to estimate the deposition efficiency (DE) by comparing the mass feed rate to the mass gain of the substrate. After an optimization of the feeding gas flow, powders were fed with a constant Ar flow rate of 5 slpm. Particle in-flight diagnostics were performed with the DPV-2000 system (TECNAR Automation Ltd., St-Bruno, Qc, Canada).

Following the coating experiments, each substrate was cut and metallographical cross sections were prepared. Cross sections were firstly characterized by confocal laser microscopy (LaMi) to determine the porosity and the thickness of each coating. Five LaMi images were recorded at a magnification of $\times 50$ and then analyzed via ImageJ. The Vickers hardness of the coatings was determined on the cross sections by using a Leitz Miniload 2 with an applied force of 3 N (HV0.3) for 30 s. At least five indentations were characterized per coating.

The linear thermal expansion was measured with a dilatometer (Netzsch, DIL 402C). Free-standing coatings

Table 1 List of the commercial, com, and experimental, exp, powders

Abbreviation	Type	Manufacturing process	Composition Al ₂ O ₃ /MgO	Size fraction, D10/D50/D90
028as-a1	exp	Agglomerated & sintered	28/72	12/19/30
028as-a2	exp	Agglomerated & sintered	28/72	23/35/54
052fc-a	exp	Fused & crushed	52/48	10/18/28
072ac-a	exp	Agglomerated & calcined	72/28	20/29/43
072fc-a1	com	Fused & crushed	72/28	15/28/43
072fc-a2	com	Fused & crushed	72/28	10/17/26
076as-a	com	Agglomerated & sintered	76/24	22/38/63
076as-b	exp	Agglomerated & sintered	76/24, 3TiO ₂	23/31/41
094fc-a	exp	Fused & crushed	93,5/6,5	12/21/36

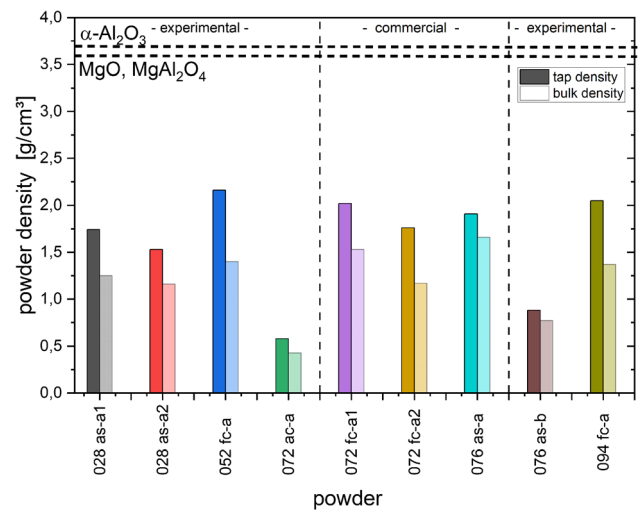
The abbreviations show the weight content of Al₂O₃, the manufacturing process, and a letter for the manufacturer, a number for the size fraction. The powders listed in bold were used for the DOE

Table 2 DOE parameters used in the present investigation

Powder	Current, A	H ₂ /Ar – ratio, slpm	Stand-off distance, mm
072fc-a1	540-620-700	2/48-7/43-12/38	80-110-140
076as-a	540-620-700	2/48-7/43-12/38	80-110-140
094fc-a	480-590-700	2/48-7/43-12/38	80-140-200

were cut to sizes of 3*25mm² and measured in air from room temperature to 1200 °C with a heating rate of 3 K/min. The mean value over this temperature range is given as result.

The samples for thermocycling tests were sprayed on austenitic chrome nickel steel (1.4841, German material number) substrates. These were coated with a NiCr bond coats (Ni 105, Praxair) using an gas-fuelled HVOF process (DJ2700, Oerlikon). In the thermocycling test, the samples were hold for one cycle of 20 h at 950 °C in air with a fast cooling rate using compressed air from the coating side or with slow cooling rate in the furnace. As we also wanted to investigate the effect of cooling rates on the performance of the coatings, even faster cooling rates have been used in an additional test (thermal shock test). Coated substrates were put in the preheated furnace (950 °C) using SiSiC porous substrates. Then, the samples were kept in the furnace for 15 to 30 min to reach the furnace temperature. After reaching the furnace temperature, samples were taken out of the furnace within about 2 s and cooled down using a ventilator or water (20–24 °C). After the tests water immersed samples were dried in a furnace at 100 °C for 15 min before repeating the cycle. After each cycle samples were inspected and damage recorded.

**Fig. 1** Densities of the used powders

Results and Discussion

Bulk and tap densities of the used powders are given together with the theoretical densities of MgO, MgAl₂O₄ and Al₂O₃ in Fig. 1. The densities were in the range between 1.2 and 1.7 g/cm³ for bulk and 1.5 to 2.2 g/cm³ for tap density, respectively. Two exceptions were the powders 072ac-a and 076as-b which showed densities below 1 g/cm³. Both powders showed in a cross section a large amount of internal porosity due to the manufacturing process. Figure 2 gives the result of the phase analysis of the powders. As expected, the results show a reduced MgO

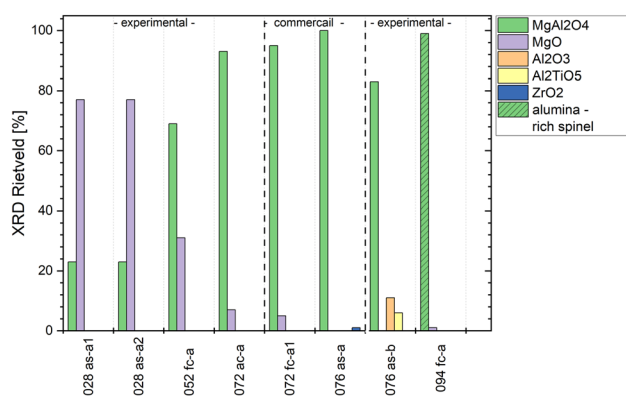


Fig. 2 Phase evaluation of the used powders (072fc-a1 corresponds to 072fc-a2)

content with increasing Al₂O₃ content. In the experimental powder 076as-b TiO₂ was added to achieve an improvement in spray processing as a result of the decrease of the sintering temperature of about 200 °C. This led to the formation of aluminum titanate. In 094fc-a only a cubic phase (*Fd-3 m*) was found. The lattice parameter ($a = 7.947 \text{ \AA}$) of 094fc-a determined by Rietveld refinement is in a better agreement with that of the γ -alumina (Al_{2.67}O₄, ICSD 603,780; $a = 7.947 \text{ \AA}$) as for MgAl₂O₄, (ICSD 31,373; $a = 8.081 \text{ \AA}$).

In Fig. 3, the contour plots of the performed DOE are shown which give the deposition efficiencies as function of two of the three parameters varied according to Table 2. It is obvious that for the chosen parameter sets, the H₂/Ar ratio has the largest effect. The higher efficiency with increased hydrogen content is well known. It is due to the arc constriction for larger hydrogen contents leading to higher voltages at constant power. As heat loss is mainly dominated by the current, this enhances the efficiency of the process (Ref 17). Of course, also the higher enthalpy of the plasma for higher hydrogen ratios in combination with the high thermal conductivity of hydrogen leads to a better heat transfer to the particles, higher degree of melting and hence, a higher deposition efficiency. Also, the increasing current leads to an increased deposition efficiency, and however, the extent is in the given parameter range rather limited. The lowest impact has the stand-off distance, between 80 and 140 mm for the 072fc-a1 and the 076as-a powders. The impact is rather marginal. For the alumina-rich 094fc-a powder, the parameter regime was increased, here a slightly larger effect is visible. In general, deposition efficiency decreases with stand-off distance as the jet cools down and decelerates by entrapment of air. This effect could be measured by DPV diagnostics showing for the 072fc-a1 and 076as-a powders a temperature decrease from 2870 to 2700 °C and a velocity decrease from about

300 m/s to 260 m/s. Obviously, these decreases are too low to have a distinct impact on the deposition efficiency.

For one powder, 072fc-a1, the influence of the gun power on efficiency (a), hardness (b), and porosity (c) is shown (Fig. 4). It is expected that the deposition efficiency increases with power. However, Fig. 4(a) shows clearly distinct regimes for each H₂/Ar value. All different H₂/Ar results fall more or less on the same line. This is by far not so clearly visible for the hardness values, here just an increase with power level is observed (Fig. 4b). For the porosity levels, a rather large scatter of the data is observed (Fig. 4c), that was also the reason why the corresponding contour plots were not shown. Although the procedures of metallographic preparation and corresponding image analysis have been standardized, the data seem to be less reliable. Anyhow, also here all the data follow a drop of porosity with increasing power with no distinct steps according to the H₂/Ar ratio.

In the plots of Fig. 4, the gross power levels are given. As mentioned earlier, the efficiency should increase with increasing hydrogen levels, as one would expect an increased enthalpy in the plasma flame for higher hydrogen contents. This together with the better heat transfer in a hydrogen-containing gas could explain the higher deposition efficiency. On the other hand, the nearly linear dependence of hardness and in part porosity on the power level — without sharp steps for varied H₂/Ar ratios — appears not in line with this finding. A possible explanation could be that the heating of the feedstock is changed in a way that more particles are (partially) molten (increasing efficiency); however, these properties in the mean do not generate denser coatings (leading to lower porosity or higher hardness). As it is known that typically hydrogen increases the velocity of the plasma and the particles, the dwell time and, hence the heating, is reduced. A similar effect has the reduced plasma temperature in a hydrogen plasma. However, DPV measurements indicate a reduced velocity and rather constant temperatures with increasing hydrogen amount. Although it is not in line with typical findings in the literature, it could also lead to similar coating properties at different H₂/Ar ratios.

From the DOE results, a parameter set was selected which gave the best properties with respect to deposition efficiency, hardness, and porosity. This parameter set was a current of 700 A and a H₂/Ar ratio of 0.3158 resulting in a power of 47.2 kW. To keep the substrate temperature below 250 °C, a stand-off distance of 110 mm was chosen. For these parameters, the calculated and the measured values, *DE* 50.3%/49.0%, porosity 10.7%/9.1%, HV0.3 908.3/907.5, respectively, were in very good agreement. The micrographs of the coatings from the different powders sprayed with this set are shown in Fig. 5. The deposition efficiencies of the powders were in the range

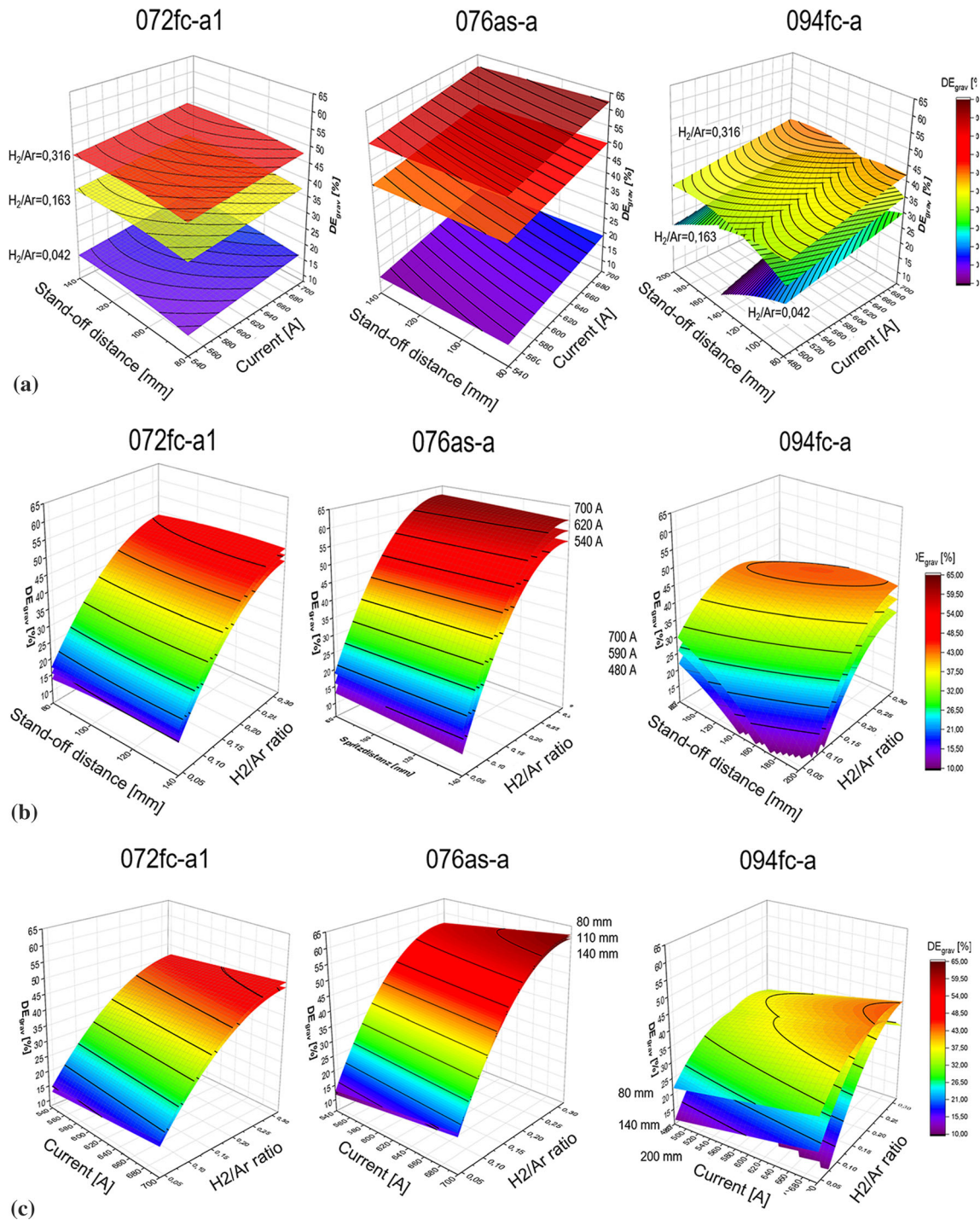


Fig. 3 The contour plots of the DOE for the dependence of deposition efficiency on stand-off distance/current (a), stand-off distance/ H_2 to Ar ratio (b), and current/ H_2 to Ar ratio (c) for selected powders

between 47 and 59% with the exception of powder 072fc-a2 for which a value of 28% was determined. This might be related to the fine particle size and a non-optimal penetration in the plasma plume. However, it is unclear why this was not observed for the 052fc-a powder which had a similar particle size. The low efficiency led to a rather low

coatings thickness of 170 μm using 10 passages. Also for the powder 072ac-a only a low thickness of 230 μm was obtained for the same conditions, in this case due to the lower powder density (see Fig. 1). The typical coating thickness of the other powders used for the further investigations was about 400 μm .

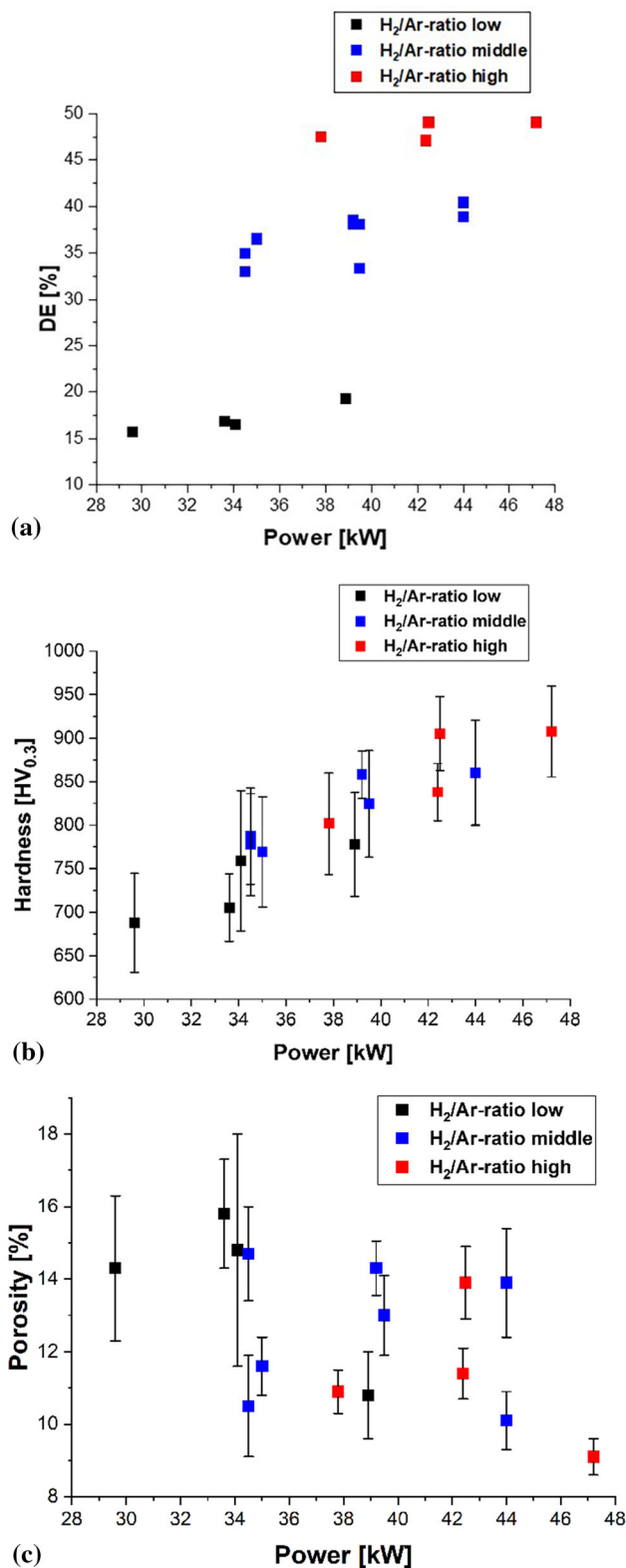


Fig. 4 Deposition efficiency (a), hardness (b), and porosity (c) as a function of the gun power for the powder 072fc-a1

XRD results of several of the coatings are presented in Fig. 6. As expected, coatings from the MgO-rich powders have a binary phase composition consisting of MgO and spinel, and coatings from MgO lean powders show mainly the γ -alumina phase. For the near stoichiometric powders, the spinel phase is dominant.

It should be pointed out that a quantitative evaluation of the XRD patterns was due to surface effects, unknown amounts of amorphous phase and strong texturing difficult. So, the results presented in Fig. 6 have to be treated with care. In addition, also the similarity of the crystal structures of γ -alumina and $\text{Mg}_{1-x}\text{Al}_{2+x}\text{O}_{4-x}$ ($0 \leq x \leq 1$) can result in further uncertainties. It has also to be stated that in the coating 028as-a1 the MgO phase contains a rather large amount of substoichiometric Mg_{1-x}O . A further outcome of the investigation is that in the alumina-rich coating (094fc-a) mainly γ -alumina is present. In all coatings, no α -alumina was found.

The porosity values of the different coatings are shown in Fig. 7(a) and were in the range between 4 and 12%. It has to be pointed out that not all the visible gray areas are due to porosity but show a second phase. Only the black regions are due to porosity. However, this is not always clearly distinguishable and leads to the rather large error bars in Fig. 7(a). In Fig. 7(b), hardness values are plotted. Often a clear relation between porosity and hardness is found in thermally sprayed, single-phase coatings. However, here the relation is not so clear mainly because of different phases in the coatings. In the literature, the stated hardness values of sintered ceramics show a certain variation as density, impurity contents and grain size influence the results. For comparison, we will here use the compilation of McColm (Ref 18) giving HV values for MgO in the range between 500 and 1000, for MgAl_2O_4 from 1200 to 1700 and for α -alumina 1800 to 2300. In as-sprayed coatings typically only γ -alumina is present (as it is found here, too), however, no data on the hardness of highly dense, sintered samples are available as the material would transform into α -alumina. The values of dense, thermally sprayed coatings can be as high as 1500 (Ref 19). These hardness values together with the porosity data (Fig. 7a) can give a reasonable explanation of the hardness data in Fig. 7(b). Starting with the three 072 powders (rather pure spinel phase), their hardness values show a clear relation to the porosity levels. The samples from powders with higher than stoichiometric alumina content have a rather higher density. However, the hardness values do not exceed the value of the densest spinel coatings. This might be explained by a reduced hardness of the alumina-rich spinels due to the higher amount of cation vacancies (Ref 4) and the reduced hardness of the γ -alumina phase. Also, the TiO_2 content of 3% in the coating from the 076as-b powder might reduce the hardness. For the MgO-rich samples

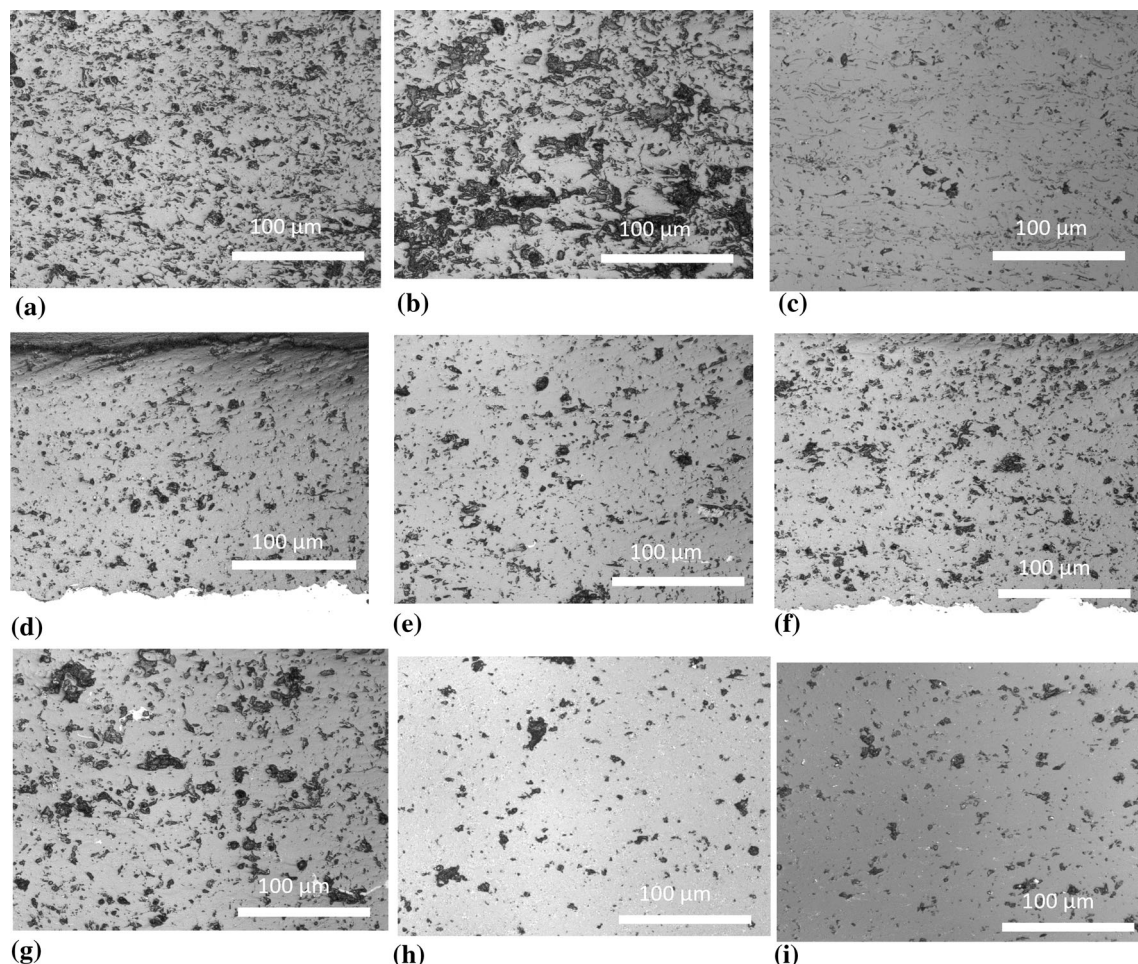


Fig. 5 Laser microscope images of coatings of the powders sprayed with the identified optimal conditions, the figures (a)–(i) correspond to the powders 028as-a1 to 094 fc-a (s. Table 1)

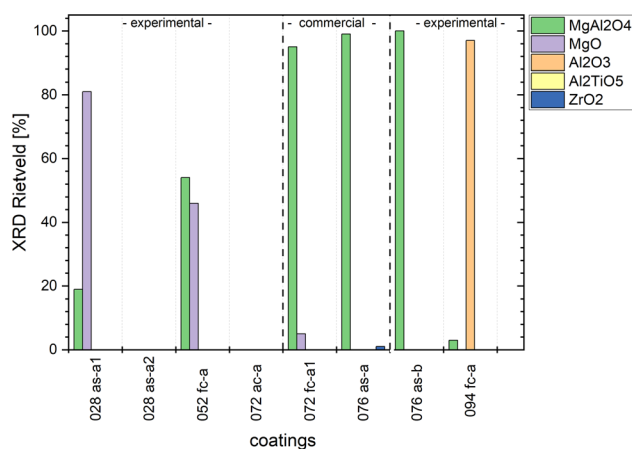


Fig. 6 Estimated phase analysis results (see text) of several of the sprayed MgO/Al₂O₃ coatings

again high densities were found with moderate hardness values. This can be attributed to the reduced hardness of the MgO phase.

In addition to the hardness values, the paper also presents results on thermo-mechanical testing. For the interpretation of these results also the thermal expansion coefficients (TECs) are important, as they often dictate the developing thermal stress levels.

For a sample sprayed from 028as-a1 (MgO-rich) between 60 and 1200 °C, a mean TEC value of $12.9 \cdot 10^{-6}/\text{K}$ was determined, while the rather stoichiometric powder (072fc-a2) gave a value of $9.7 \cdot 10^{-6}/\text{K}$. These results are expected due to the high thermal expansion coefficient of MgO compared to the one of Al₂O₃. In the literature values of $12\text{--}13 \cdot 10^{-6}/\text{K}$, $8.3 \cdot 10^{-6}/\text{K}$ and $8.0\text{--}8.3 \cdot 10^{-6}/\text{K}$ are found for the mean linear thermal expansion coefficient between room temperature and 1000 °C for MgO, MgAl₂O₄ and Al₂O₃, respectively (Ref 20).

In Fig. 8, the spinel coatings in the as-sprayed condition and after one and two cycles for slow (right) and fast (left) cooling (cooling from the coating side) are shown. For the fast cooling from the coating surface the coatings with intermediate alumina content (expansion coefficients

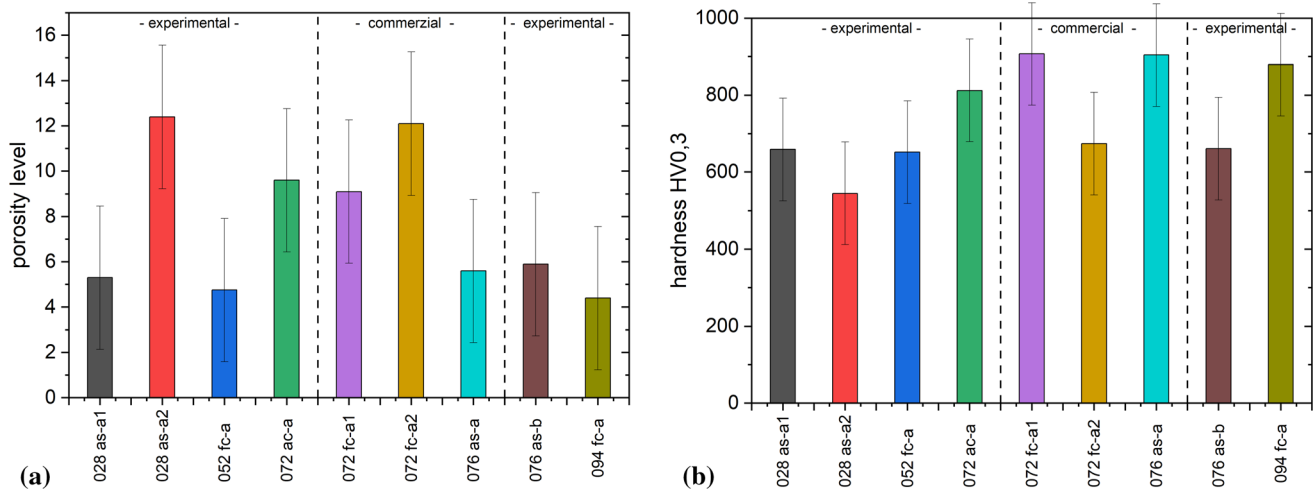
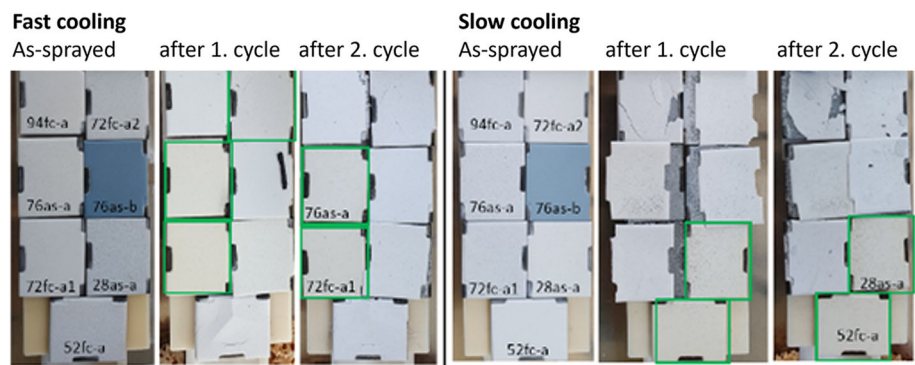


Fig. 7 Porosity levels (a) and hardness results (b) of coatings sprayed from the different powders

Fig. 8 Photos of the different samples as-sprayed (1. and 4. column), after the first cycle (2. and 5. column) and after the second cycle (3. and 6. column). The left 3 columns correspond to fast, the right ones to slow cooling. Marked with green squares are the samples which survived. The top row shows industrial spinel coatings also tested



expected in the range between 8.0 and $8.3 \cdot 10^{-6}/\text{K}$ survived, while for the slow cooling rates, the MgO-rich coatings performed better. This can be explained considering the stresses developing in such coatings. If the cooling is made fast from the coating side, the stresses develop due to the cooling of the coating while the substrate remains rather hot and does hardly contract. Here, the thermal expansion of the coating determines the stress level, it should be as low as possible (so Al_2O_3 -rich). That the 094fc-a coating did not survive the second cycle might be due to microstructural features as a high amount of γ -alumina with poor mechanical properties. On the other side, if coating and substrate are cooled down slowly and hence simultaneously, the mismatch of thermal expansion coefficients determines the stress, hence a high expansion coefficient of the coating (high MgO content) is beneficial.

In the thermal cycles with water cooling, in which both substrates and coatings are cooled simultaneously, the coatings with high MgO again performed best. Due to the simultaneous cooling of substrate and coating, the thermal expansion mismatch is determining the stress level, and hence, the coatings with a high coefficient perform best.

Summary

Three different $\text{MgO}/\text{Al}_2\text{O}_3$ powders have been used for performing DOE experiments with H_2/Ar ratios, current, and stand-off distance as parameters. In the given parameter range, the H_2/Ar ratios had the largest impact on the deposition efficiency, followed by the gun current and the stand-off distance.

Interestingly, an increase of the hydrogen content leads to a significant increase of the deposition efficiency, while no significant increase of the coating properties at a similar power level was observed. A possible explanation is given in the paper.

From the DOE, an optimized parameter set was determined and used for all different powders which were in detail characterized within the project. Here, the results of porosity values, hardness and thermal cycling tests were presented. For test conditions with first cooling of the coating, a low thermal expansion coefficient appears favorable (high alumina content). If substrate and coating are cooled simultaneously, a high TEC (low mismatch) is beneficial.

Acknowledgments The IGF-project Nr.: 20620 BG / DVS-Nr.: 02.2265 of the Forschungsvereinigung Schweißen und verwandte Verfahren e.V. of the DVS, Aachener Str. 172, 40223 Düsseldorf, was funded via AiF within the frame of a program for the funding of the industriellen Gemeinschaftsforschung (IGF) of the Bundesministerium für Wirtschaft und Energie based on a decision of the German parliament. The commercial powders were supplied by Saint Gobain Ceramic Materials GmbH and Ceram GmbH Ingenieurkeramik. Several experimental powders were delivered by Saint Gobain. Furthermore, the authors would like to thank the technicians, Ralf Kurze, Karl-Heinz Rauwald, Sigrid Schwartz-Lückge, and Dr. Yoo Jung Sohn, all at Forschungszentrum Jülich GmbH, for performing the spraying experiments, several hardness measurements, and support of the XRD analysis.

Funding Open Access funding enabled and organized by Projekt DEAL.

Open Access This article is licensed under a Creative Commons Attribution 4.0 International License, which permits use, sharing, adaptation, distribution and reproduction in any medium or format, as long as you give appropriate credit to the original author(s) and the source, provide a link to the Creative Commons licence, and indicate if changes were made. The images or other third party material in this article are included in the article's Creative Commons licence, unless indicated otherwise in a credit line to the material. If material is not included in the article's Creative Commons licence and your intended use is not permitted by statutory regulation or exceeds the permitted use, you will need to obtain permission directly from the copyright holder. To view a copy of this licence, visit <http://creativecommons.org/licenses/by/4.0/>.

References

1. I. Ganesh, A Review on Magnesium Aluminate (MgAl_2O_4) Spinel: Synthesis, Processing and Applications, *Int. Mater. Rev.*, 2013, **58**(2), p 63–112.
2. H. Eschnauer, K. Mundinger, H. Kühn, and O. Stitz, Pulverförmige Keramische Werkstoffe zum Plasmaspritzen, *Ber. Dtsch. Keram. Ges.*, 1980, **57**, p 94–98.
3. U. Bast and E. Schuhmann, Development of novel oxide materials for TBC's, 26th Annual Conference on Composites, Advanced Ceramics, Materials, and Structures: B: Ceramic Engineering and Science Proceedings, 2002. p 525–32
4. N. Schlegel, S. Ebert, G. Mauer, and R. Vaßen, Columnar-Structured Mg-Al-Spinel Thermal Barrier Coatings (TBCs) by Suspension Plasma Spraying (SPS), *J. Therm. Spray Technol.*, 2015, **24**(1), p 144–151.
5. T. Steinke, G. Mauer, R. Vaßen, D. Stöver, D. Roth-Fagaraseanu, and M. Hancock, Process Design and Monitoring for Plasma Sprayed Abradable Coatings, *J. Therm. Spray Technol.*, 2010, **19**, p 756–764.
6. S. Ebert, T. Steinke, R. Vaßen, and D. Stöver, Failure mechanism of non-stoichiometric Mg-Al-Spinel abradable coatings under thermal cyclic loading, International Thermal Spray Conference and Exposition 2011 (ITSC 2011) Hamburg, DVS-Berichte, DVS Media, Düsseldorf, Germany, 2011, 27092011 - 29092011
7. E.H. Lutz, Plasma Ceramics - Properties and Applications, *Cfi/Ber DKG.*, 1997, **74**(3), p 148–151.
8. C. Petot, M. Ducos, and G. Petotervas, Thermal Spray Spinel Coatings on Steel Substrates - Influence of the Substrate Composition and Temperature, *J. Eur. Ceram. Soc.*, 1995, **15**(7), p 637–642.
9. H. Grütznier and H. Weiss, Development of ceramic plasma sprayed coatings against slag attack for the steel industry, *Advances in Thermal Spraying*. C.C. Berndt Ed., Pergamon Press, Montreal Canada, 1986, p 349
10. M. Nakamichi, K. Miyajima, Y. Harada, and R. Oyamada, Trial Fabrication and Preliminary Characterization of $\text{MgO}/\text{Al}_2\text{O}_3$ Coating, *J. Nucl. Mater.*, 1996, **233–237**, p 1427–1430.
11. P. Varghese, Long-Term Exposure of MgAl_2O_4 and Y_2O_3 Thermal Barrier Coatings in Molten Sodium, *Surf. Coat. Technol.*, 2020, **381**, p 125111.
12. L. Brown and R.K. MacCrone, *Advances in Thermal Spraying*, Pergamon Press, Canada Montreal, 1986.
13. K. Ahn, B.W. Wessels, and S. Sampath, Spinel Humidity Sensors Prepared by Thermal Spray Direct Writing, *Sens. Actuators B Chem.*, 2005, **107**(1), p 342–346.
14. M. Niittymäki, K. Lahti, T. Suhonen, U. Kanerva, and J. Metsäjoki, Ed., Influence of humidity and temperature on the dielectric properties of thermally sprayed ceramic MgAl_2O_4 coatings, 2014 IEEE Conference on Electrical Insulation and Dielectric Phenomena (CEIDP), 2014
15. J. Arnold, S.A. Ansar, U. Maier, and R. Henne, Insulating and sealing of SOFC devices by plasma sprayed ceramic layers, *Conference Proceedings-CD*. B.R. Marple, Y.-C. Lau, C.-J. Li, R.S. Lima, G. Montavon Ed., Springer, Maastricht Netherlands, 2008, p 95–99
16. G. Lallemand, S. Fayeulle, D. Treheux, and C. Esnouf, Microstructure study of spinel plasma coatings, *ITSC 1998*. C. Coddet Ed., ASM International, Nice France, 1998, p 599–604
17. P. Pfauchais, J. Herberlein, and M. Boulos, *Thermal Spray Fundamentals*, Springer, New York, 2014.
18. I.J. McColm, *Ceramic Hardness*, Springer, New York, 1990.
19. Y. Gao, X.L. Xu, Z.J. Yan, and G. Xin, High Hardness Alumina Coatings Prepared by Low Power Plasma Spraying, *Surf. Coat. Technol.*, 2002, **154**(2–3), p 189–193.
20. R. Morrell, *Handbook of Properties of Technical & Engineering Ceramics, Part1 An Introduction for the Engineer and Designer*, HMSO Publications Centre, London, 1985.

Publisher's Note Springer Nature remains neutral with regard to jurisdictional claims in published maps and institutional affiliations.